Applied Catalysis B: Environmental 202 (2017) 262–268

Contents lists available at ScienceDirect

Applied Catalysis B: Environmental

journal homepage: www.elsevier.com/locate/apcatb

Catalytic supercritical water gasification: Interaction of sulfur with ZnO and the ruthenium catalyst

G. Peng[a], C. Ludwig[a,b], F. Vogel[a,c,*]

[a] Energy and Environment Research Department, Paul Scherrer Institut (PSI), 5232 Villigen PSI, Switzerland
[b] ENAC-IIE, Ecole Polytechnique Fédérale de Lausanne (EPFL), 1015 Lausanne, Switzerland
[c] University of Applied Sciences Northwestern Switzerland (FHNW), 5210 Windisch, Switzerland

ARTICLE INFO

Article history:
Received 7 July 2016
Received in revised form 26 August 2016
Accepted 3 September 2016
Available online 4 September 2016

Keywords:
Methane
Ruthenium on carbon
Zinc oxide
Sulfur poisoning
Catalytic supercritical water gasification

ABSTRACT

Continuous catalytic supercritical water gasification (CSCWG; 400 °C, 28 MPa) of microalgal biomass (*Chlorella vulgaris*) was carried out at the microalgae production site of ZHAW in Wädenswil (Switzerland) non-stop over a period of 100 h. Characterization of the spent catalyst showed that mainly sulfur poisoning, and to a lesser extent coking, salt deposits, and some sintering of the Ru nanoparticles were responsible for the deactivation of the catalyst after 55 h of time on-stream. The commercial zinc oxide adsorbent exhibited a high mechanical stability and good sulfur adsorption performance under supercritical water conditions although its specific surface area collapsed. In summary, the use of a zinc oxide adsorbent upstream of the catalyst bed, together with a higher ruthenium loading of the catalyst, improved the long-term performance of the CSCWG process significantly.

1. Introduction

Catalytic supercritical water gasification (CSCWG) uses the unique properties of supercritical water (T > 374 °C, p > 22.1 MPa) for decomposing wet biomass (*e.g.* microalgae, manure, sewage sludge) into gaseous products (CH_4, H_2, CO_2, and CO). This technology is well suited for processing microalgae since no drying step is needed allowing to reach high thermal efficiencies (70–77%) with short residence times (< 30 min) [1]. At low to moderate temperatures (T < 500 °C), metal-supported catalysts are required for achieving high gasification rates and a high CH_4 selectivity. The choice of the catalyst relies mainly on the gaseous fuels wished (CH_4 or H_2). In Fig. 1, the desirable catalytic properties for CH_4 production are shown.

Biomass is first hydrolyzed into small aliphatic molecules such as acetic acid, formic acid, and acetaldehyde, which can diffuse to the catalytic active sites [5]. These intermediate products decompose on the catalyst surface through C—C bond cleavage resulting in the formation of H_2 and CO, which are further upgraded via the water-gas shift (WGS) reaction into CO_2 and H_2. If the catalyst favors the cleavage of C—O bonds, the produced H_2 is used for the hydrogenation of the adsorbed species resulting in the formation of CH_4. Hence, if the target product is CH_4, the catalyst should exhibit a high activity for the cleavage of C—C and C—O bonds and enhance the WGS reaction. For H_2 production, the catalyst should minimize the cleavage of C—O bonds, besides favoring the cleavage of C—C bonds and the WGS [6,7]. Ru was found to be the most active and selective metal towards CH_4 formation due to its ease for favoring the cleavage of C—O bonds [5]. Osada et al. [8] found that Ru was the most active metal compared to other metals (Rh, Pt, Pd, and Ni) during CSCWG of lignin at 400 °C and 37.1 MPa. The choice of the catalyst support is crucial, especially when working under the harsh conditions of SCW. Only α-Al_2O_3, *monoclinic*-ZrO_2, *rutile*-TiO_2, and carbon were reported to be stable [9–12]. In a previous study [13], we compared the catalytic performance of several supported Ru catalysts during continuous CSCWG of isopropanol (450 °C, 30 MPa) over a period of 50 h. The catalyst stability was in the order of: Ru/C > Ru/*monoclinic*-ZrO_2 > Ru/α-Al_2O_3 ≈ Ru/*rutile*-TiO_2. The high Ru dispersion achieved on the Ru/C was beneficial for the improvement of the catalyst stability due to the higher gasification rate versus the coke formation rate.

The low sulfur tolerance of Ru-supported catalysts is a major concern for the technology development. Haiduc et al. [14] were the first to assess the effect of sulfur during CSCWG of microalgae (*Phaeodactylum tricornutum*) (400 °C, 30 MPa) over a 2% Ru/C catalyst in a batch reactor. By increasing the sulfur-to-catalyst ratio, they observed a decrease of the carbon gasification effi-

* Corresponding author at: Energy and Environment Research Department, Paul Scherrer Institut (PSI), 5232 Villigen PSI, Switzerland.
E-mail address: frederic.vogel@psi.ch (F. Vogel).

http://dx.doi.org/10.1016/j.apcatb.2016.09.011
0926-3373/

ciency (GE_C) demonstrating the negative effect of sulfur on the catalyst performance. In a similar work performed by Guan et al. [15] the same trend was reported when gasifying *Nannochloropsis* sp. (410 °C) over a 5% Ru/C catalyst. During continuous CSCWG of *Phaeodactylum tricornutum* (420 °C, 32 MPa) over a 2% Ru/C catalyst, Bagnoud-Velásquez et al. [16] observed a fast deactivation of the catalyst caused mainly by sulfur poisoning, coking, and salt deposits. Hence, in order to achieve high periods on stream, there is a need to develop sulfur-resistant catalysts, regeneration methods, and/or sulfur removal methods. Waldner [17] has poisoned a 2% Ru/C catalyst on stream with Na_2SO_4 under SCW conditions. The regeneration was performed with 1 wt% H_2O_2 at 50 °C during 3 h and at 90 °C for an additional 3.3 h. During the first hours, the catalytic activity was almost totally recovered with a gas composition similar to the thermodynamic chemical equilibrium. After 24 h on stream, the total organic carbon conversion dropped steadily up to 80%. This loss was explained by a too short regeneration period. More recently Dreher et al. [18] optimized the regeneration method proposed by Waldner and investigated *in situ,* using X-ray Absorption Spectroscopy, the structural change of Ru under reaction conditions. After being sulfur poisoned with dimethyl sulfoxide, the catalyst was regenerated with H_2O_2 at different temperatures (75–125 °C) and regeneration times (20–240 min). Extended X-ray absorption fine structure measurements revealed that S-Ru/C was entirely oxidized and converted to RuO_2/C suggesting that the sulfur species were removed from the Ru surface. After the reductive pre-treatment with ethanol, the catalytic performance of the regenerated catalyst was similar to the fresh one during CSCWG of ethanol (390 °C, 24.5 MPa). Similarly to Waldner's experiment, a decrease of the catalytic activity was observed after a few hours on stream. The change of the Ru NPs size and structure following the oxidative pre-treatment has been proposed to be responsible for the activity loss. Besides regeneration methods, continuous sulfur removal with a sulfur adsorbent material has been reported by Elliott et al. [19] during continuous hydrothermal gasification (350 °C, 20 MPa) of different microalgae species (*e.g. Spirulina, Nannochloropsis salina*). A sulfur scrubber bed (Raney nickel) was implemented upstream of the catalytic reactor. Their results showed the low effectiveness of Raney nickel for removing sulfur. In a recent work [20], we reported continuous CSCWG of *Chlorella vulgaris* (400 °C, 28 MPa) over a 5% Ru/C catalyst. The experiment was carried out at the microalgae production site of ZHAW in Wädenswil (Switzerland) non-stop over a period of 100 h. A sulfur removal unit, using a commercial ZnO adsorbent material, has been implemented upstream of the catalyst. Chemical analysis of the reactor effluent suggested that sulfur was adsorbed during a period of 60 h. As a result, microalgae were successfully gasified to a methane-rich gas during 55 h. However, no characterization of both the spent catalyst and sulfur adsorbent were performed in order to understand the deactivation causes of the catalyst and the sulfur adsorption performance of ZnO. In this work, a thorough analysis of the spent catalyst and ZnO adsorbent used during the gasification campaign are presented.

2. Methods and materials

2.1. Experimental setup

Continuous CSCWG was carried out with a catalytic reactor system (KONTI-C) having a feed capacity of 1–2 kg h^{-1} described in detail elsewhere [20]. The plant consists of six main sections: feeding section, salt separator, salt removal section, reactor, pressure control and release, phase separator. The lower part of the reactor was filled with 713 g (on a wet basis, 5.2 wt% H_2O) of a commercial ZnO adsorbent (*Johnson Matthey Catalysts, KATALCO 32-5*) with a diameter of 2.8–4.8 mm and containing 60–100 wt% of ZnO, and the upper part was filled with 493 g (on a dry basis) of a commercial 5% Ru/C catalyst (*BASF*).

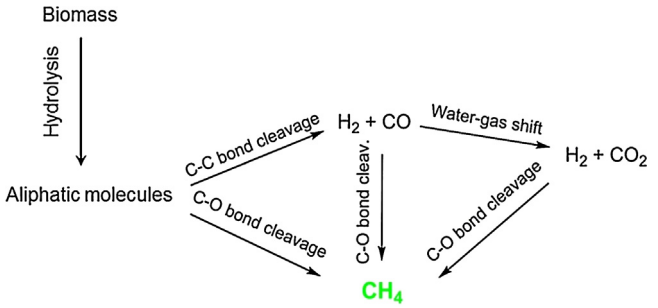

Fig. 1. Reaction pathways for CH_4 production during CSCWG of aliphatic molecules. (taken from Ref. [2], adapted from Refs. [3,4]).

2.2. Characterization methods

The elemental analysis of the feedstock was performed at ETH Zürich (Microelemental Analysis Laboratory). The following analyzers were used: carbon, nitrogen, hydrogen (LECO CHN-900), oxygen (LECO RO-478), sulfur (LECO CHNS-932), phosphorus (photometer), chloride (ion chromatography). The ash content of the feedstock was determined by temperature-programmed oxidation (TPO). The sample was heated to 900 °C under flowing O_2/Ar (10:90, 10 mL min^{-1}). The carbon and sulfur elemental analysis of the ZnO adsorbent were performed with an elemental analyzer (*Vario EL cube, Elementar*). Elemental analysis of the catalyst was carried out with wavelength dispersive X-ray fluorescence (WDXRF) spectroscopy (*S4 Explorer, Bruker AXS*). Prior to the analysis, the samples were dried in a vacuum oven at 60 °C and 0.02 MPa during 2 h. Then, the samples were mixed with boric acid in a mortar and pressed to obtain a solid pellet. For the CO pulse chemisorption, the samples were reduced under H_2/Ar (10:90, 20 mL min^{-1}) at 450 °C for 4 h to clean the ruthenium surface from any deposited carbon species. Then it was flushed by pure He at 450 °C for 1.5 h for removing adsorbed H_2 from the catalyst, and finally cooled down to room temperature (RT). The CO pulses were carried out with CO/He (20:80, 40 mL min^{-1}) at RT. The dispersion was calculated by assuming 1 as the stoichiometric factor for CO:Ru. The following formula was used for determining the dispersion:

$$D_{CO} = \frac{N_{ads} \cdot F_S \cdot M_{met} \cdot 0.1}{w_{met}} \quad (1)$$

where N_{ads} is the amount of gas adsorbed in pulse chemisorption (mmol g^{-1}); F_s corresponds to the stoichiometric factor (moles of metal/mol of gas = Ru:CO); M_{met} is the metal atomic weight (g mol^{-1}) and w_{met} is the metal loading of the catalyst (wt%). The N_2-physisorption measurements were performed with an Autosorb-1 (Quantachrome Instruments) for determining the BET specific surface area and the porosity. The total pore volume was measured at $p/p_0 = 0.99$ and the mesopore volume with the t-plot method. Prior to N_2-physisorption degassing under He at 300 °C for 6 h was carried out for all the samples. The Ru nanoparticle size (NPs) was characterized by Scanning Transmission Electron Microscopy (STEM) at ETH Zürich. The measurements were performed with an aberration corrected dedicated STEM microscope (*Hitachi HD-2700 CS*), operated at an acceleration voltage of 200 kV and equipped with a high angle annular dark field (HAADF) detector. For each sample, different areas were carefully selected in order to have a reliable representation of the average Ru NPs size. The

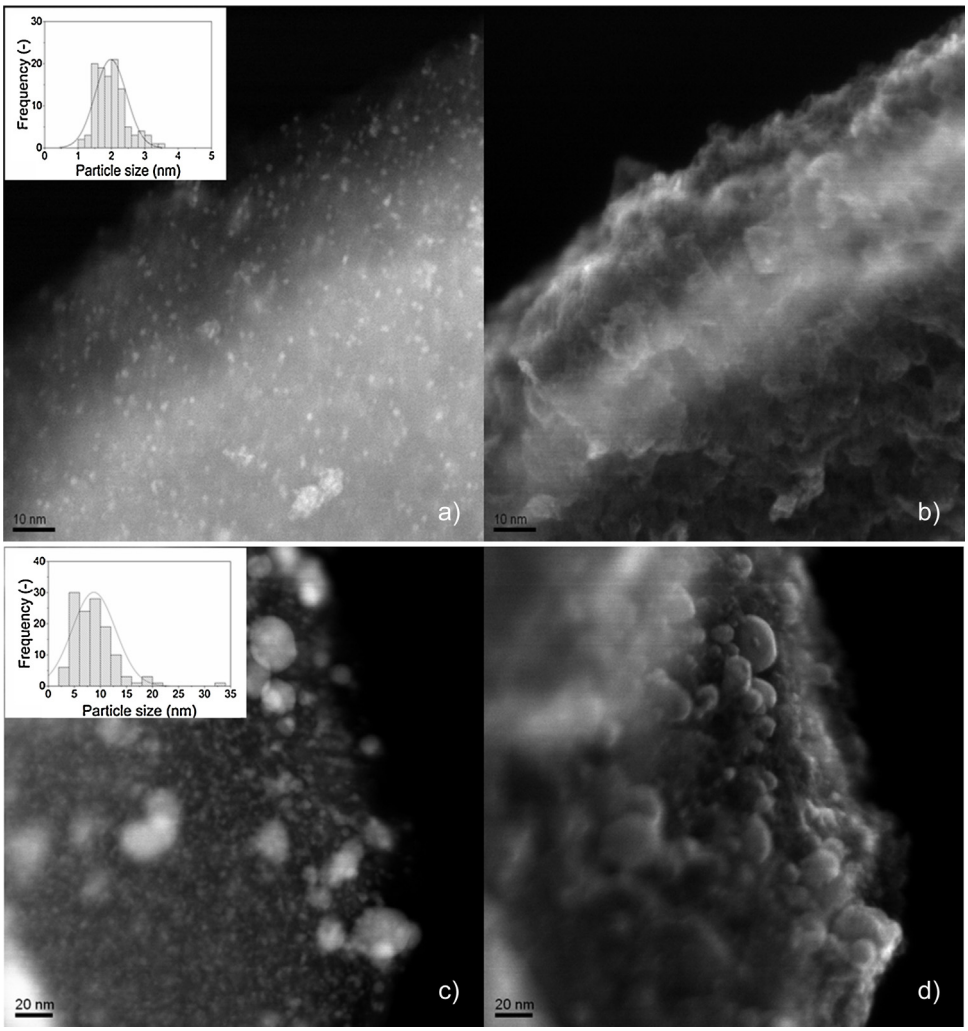

Fig. 2. HAADF-STEM images of the (a), (b) fresh and (c), (d) spent (top fraction) 5% Ru/C catalyst. The images (a) and (c) were acquired by Z contrast, whereas the images (b) and (d) by secondary electron.

average Ru NPs size and the Ru dispersion (D_{STEM}) were calculated as:

$$d_{p,STEM} = \frac{\sum_i n_i \cdot d_i^3}{\sum_i n_i \cdot d_i^2} \quad (2)$$

$$D_{STEM} = \sqrt[1.23]{\frac{d_{at} \cdot 3.32}{d_{p,STEM}}} \text{ for } 0.2 < D_{STEM} < 0.92 \quad (3)$$

$$D_{STEM} = \frac{d_{at} \cdot 5.01}{d_{p,STEM}} \text{ for } D_{STEM} < 0.2 \quad (4)$$

Where d_{at} is the atomic diameter of Ru (d_{at} = 2.6 Å) and n_i is the number of particles with diameter d_i [21]. Scanning Electron Microscopy with Energy Dispersive X-ray Spectroscopy (SEM-EDX) was carried out on a Zeiss Ultra 55 microscope at an accelerating voltage of 17 kV. Powder X-ray diffraction (XRD) measurements were performed on a D8 ADVANCE (*Bruker*) diffractometer using Cu K1 radiation (=1.5406 Å). TPO coupled to an FTIR detector (*Bruker Tensor 27*) for CO_2 and SO_2 detection (*NETZSCH STA 449C*) was used for the qualitative measurements of the coke deposits and sulfur species on the spent ZnO. For each measurement, 100 mg of sample was loaded and heated from RT to 900 °C under flowing O_2/Ar (10:90, 10 mL min^{-1}) with a ramp of 10 °C min^{-1}.

2.3. Feedstock composition

The chemical composition of *Chlorella vulgaris* is listed in Table 1.

Microalgae concentrations from 3 to 15 wt% were processed during the gasification campaign. More detailed information about the process parameters (*e.g.* feed concentration, feed rate, temperature, pressure) set during the gasification campaign are described elsewhere [20].

3. Results and discussion

3.1. Characterization of the spent Ru/C catalyst

Peng et al. [20] showed that the 5% Ru/C catalyst was able to efficiently gasify *Chlorella vulgaris* to methane (55–60 vol%) during a period of 55 h. Between 55 and 60 h on-stream they reported a rapid deactivation of the catalyst where the gas composition started to depart from the equilibrium composition. In order to understand the deactivation causes, three different fractions of the spent catalyst were collected after the gasification campaign. The bottom fraction corresponds to the lower part of the bed, which was located just downstream of the ZnO bed, whereas the top fraction was located at the reactor outlet. As shown in Table 2, the physical structure of the bottom fraction (reactor entrance) was seriously affected since almost all the BET SSA was lost. Such a decrease of

Table 1
Chemical composition of *Chlorella vulgaris* calculated on a dry matter basis.

C wt%	H wt%	N wt%	O wt%	S wt%	P wt%	Cl wt%	Ash content wt%
50.0 ± 0.3	7.1 ± 0.1	5.8 ± 0.1	33.8 ± 0.2	0.53 ± 0.04	0.65 ± 0.01	0.08 ± 0.03	3.4 ± 0.3

Table 2
Characteristics of the fresh and spent 5% Ru/C catalysts.

Catalyst	BET SSA $m^2\ g^{-1}$	$V_{microp.}$ $cm^3\ g^{-1}$	$V_{mesop.}$ $cm^3\ g^{-1}$	D_{CO} –[a]	D_{STEM} –[b]	$d_{p,STEM}$ nm[b]
Fresh Ru/C	1254	0.42	0.21	0.23	0.47	2.2 ± 0.1
Spent Ru/C bottom	56	0.00	0.11	0.01	N.A.	N.A.
Spent Ru/C middle	1064	0.33	0.28	0.03	N.A.	N.A.
Spent Ru/C top	1110	0.36	0.27	0.01	0.10	13.5 ± 0.4

[a] Determined by CO pulse chemisorption.
[b] determined by HAADF-STEM. N.A. = not available.

the BET SSA was also observed by Bagnoud-Velásquez et al. [16]. The BET SSA of the middle and the top fractions were both slightly reduced with a loss of 15% and 11% in comparison to the fresh catalyst. The catalyst support was the same as the one used in this work, and any changes of its physical structure caused by the harsh conditions of SCW was excluded since its robustness was already proven [22]. According to them, coking and salt deposits on the catalyst were the main reasons for the reduced BET SSA. In previous work [23], the stability of a Ru/C catalyst was studied during continuous CSCWG of 10 wt% isopropanol (400 °C, 30 MPa) and it was found that the pores of the catalyst were progressively filled by carbon deposits resulting in a complete loss of the porosity.

The CO-chemisorption results show that the Ru dispersion dropped considerably for the spent catalyst in comparison to the fresh catalyst. The dispersion was similar for the three fractions and close to zero proving that the catalyst bed was fully deactivated. These results are in good agreement with those reported by Bagnoud-Velásquez et al. [16] who observed a total loss of the Ru dispersion. The incapacity of Ru for adsorbing CO results in the loss of methanation. Several deactivation mechanisms may be responsible: (i) leaching of Ru, (ii) sintering of the Ru NPs, (iii) physical blockage of the pores, and/or (iv) irreversible chemical bonding on the Ru NPs. In Fig. 2, HAADF-STEM images are shown allowing us to assess the evolution of the Ru NPs size. As illustrated in Fig. 2(a), small and highly dispersed Ru NPs (2 nm) were observed on the fresh catalyst. The histogram shows a narrow distribution of the NPs size (1–3.5 nm). Although the top fraction of the catalyst bed was weakly affected by coking and salt deposits, the Ru NPs size had considerably increased with a larger distribution (2–34 nm) (see Fig. 2(c)). Hence, sintering of the Ru NPs appears to be a plausible reason for the loss of the catalytic activity. However, it remains unclear what was the cause for the growth of the Ru NPs. It is likely that either the exposure to the harsh environment of SCW and/or the chemical bonding of some contaminants coming from the feed (*e.g.* sulfur) were responsible. In Fig. 2(b) and (d), the secondary electron images reveal the presence of some spheres on the spent catalyst having a high electron density. EDX analysis confirmed that these spheres corresponded solely to Ru NPs.

The middle fraction of the spent catalyst was analyzed with SEM-EDX (see Fig. 3). Some particles having a well-defined shape deposited on the catalyst surface. Elemental mapping revealed that these particles were constituted by minerals containing Na, Ca, S, and Zn. Thus, it seems that catalyst fouling caused by the precipitation of minerals also contributed to the deactivation of the catalyst. Although the SEM-EDX mapping did not show any sulfur species bonded to Ru NPs, an interesting trend between Zn, S, and Na was observed. The fact that these three elements were located on the same particles suggests that sulfur was adsorbed on Zn. In addition,

Table 3
WDXRF analysis of the fresh and spent 5% Ru/C catalysts calculated on a dry matter basis.

Elements	Fresh	Spent bottom	Spent middle	Spent top
Ru, wt%	5.0 ± 0.1	2.0 ± 0.1	3.6 ± 0.1	4.1 ± 0.2
Zn, wt%	0.1	7.7 ± 0.4	3.8 ± 0.6	0.9
S, mg kg^{-1}	151 ± 4	1156 ± 65	1697 ± 34	1690 ± 76
Ca, mg kg^{-1}	107 ± 2	403 ± 17	311 ± 6	325 ± 15
P, mg kg^{-1}	796 ± 5	780 ± 48	673 ± 1	299 ± 3
Fe, mg kg^{-1}	162 ± 2	332 ± 12	310 ± 8	176
Cu, mg kg^{-1}	300 ± 4	647 ± 19	463 ± 13	309 ± 6
Mg, mg kg^{-1}	110	88 ± 5	222 ± 12	153 ± 9
Na, mg kg^{-1}	1396 ± 27	174 ± 4	145 ± 3	102 ± 1
K, mg kg^{-1}	284 ± 2	226 ± 2	161 ± 3	148 ± 8
Cl, mg kg^{-1}	224 ± 3	173 ± 3	158 ± 3	157 ± 5

the presence of Na indicates that the particles were likely $Na_2SO_4(s)$ which is known to have a low solubility in SCW [24].

As shown by the WDXRF analysis, the sulfur concentration on the spent catalyst was 8–11 times higher compared to the fresh catalyst (see Table 3). By assuming that all the surface Ru atoms would react with sulfur according to the sulfur-saturated catalyst phase which was reported to be $RuS_{0.33}$ [25], the quantity of adsorbed sulfur would be ca. 0.6 g. By comparing that value with the amount of sulfur detected in the catalyst bed, which was ca. 0.7 g, most of the catalyst bed was contaminated with sulfur. The Ru content was lower for the spent catalyst compared to the fresh. The fact that a concentration gradient (increasing from the bottom to the top of the bed) was measured might be due to Ru leaching and/or dilution of Ru by either deposited carbon and/or minerals. A similar concentration gradient of Ru along the catalyst bed was observed on the spent catalyst by Elliott et al. [19]. As no leached Ru was detected in the reactor effluent, it seems that the dilution of Ru by either carbon deposits and/or minerals was the reason. The dilution can also be explained by the concentration of Zn which decreases from the bottom to the top of the bed. The presence of Zn in the catalyst bed was also observed in the SEM-EDX analysis and is likely due to some attrition or dissolution of the ZnO adsorbent. Other deposited minerals coming from the feed such as Ca, Fe, Cu, and Mg were detected along the catalyst bed as well. Note that these elements were also observed on the solid residue in the salt separator [20]. Interestingly, some minerals (*e.g.* Na, P, K, and Cl) were found at a lower concentration in the spent catalyst and might have been washed out from the fresh catalyst bed during the campaign.

3.2. Characterization of the spent ZnO adsorbent

Like for the spent catalyst, three different fractions of the spent ZnO adsorbent were retrieved from the reactor after the gasifica-

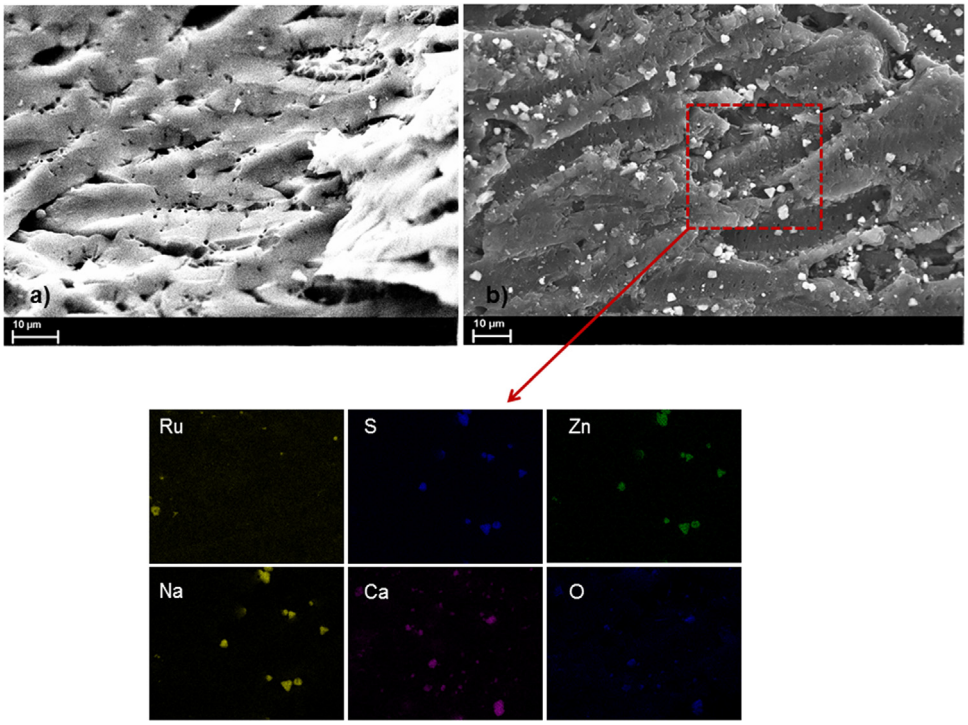

Fig. 3. SEM-EDX of the (a) fresh and (b) spent (middle fraction) 5% Ru/C catalyst.

Fig. 4. Sample of the fresh and spent ZnO adsorbents.

Table 4
Physical structure of the fresh and spent ZnO adsorbents.

Sample	BET SSA [$m^2\ g^{-1}$]	V_{total} [$cm^3\ g^{-1}$]	Average pore size [Å]
Fresh ZnO	23	0.17	151
After 18 h in SCW	4	0.05	219
Spent ZnO bottom	6	0.05	179
Spent ZnO middle	5	0.05	204
Spent ZnO top	6	0.05	163

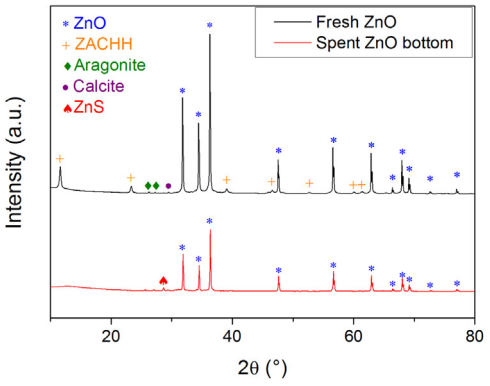

Fig. 5. X-ray diffractograms of the fresh and spent ZnO adsorbent (bottom fraction).

tion campaign. The main objectives of the *ex situ* analyses were to evaluate its macro-/microscopic stability and its sulfur adsorption performance. In Fig. 4, the samples of the fresh and spent ZnO adsorbent are shown. The macroscopic structure of the spent adsorbent and its mechanical properties were well preserved. Only a noticeable change of its color from white to gray was observed, suggesting that some chemical modifications occurred.

In order to determine the nature of these changes, N_2-physisorption, XRD, SO_2/CO_2-TPO, and carbon and sulfur elemental analysis were performed. As shown in Table 4, the physical structure of the spent adsorbent was affected in a similar manner for the three fractions. In order to evaluate the reasons for such a loss of the BET SSA, the fresh ZnO adsorbent was treated in SCW (400 °C, 30 MPa) solely with deionized water during 18 h in a fixed-bed plug flow reactor described elsewhere [23]. As the BET SSA was similarly affected for the three fractions, these changes can be attributed to the harsh conditions of SCW. The collapsing of small pores may explain the observed loss of pore volume. As a result, larger pores were formed.

According to the XRD analysis, the crystalline structure of ZnO was well preserved since the diffraction peaks of ZnO still appeared after CSCWG (see Fig. 5). The apparition of a new diffraction peak at 28.7° can be attributed to the formation of ZnS which confirms that sulfur was chemically bound to the adsorbent. The other diffrac-

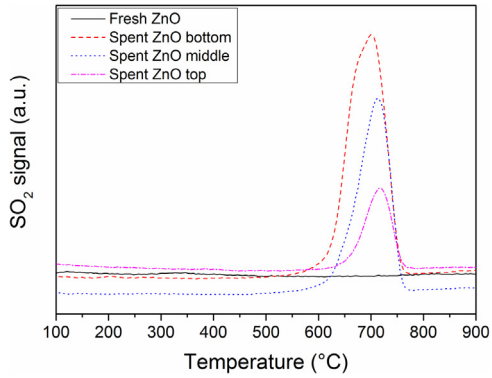

Fig. 6. SO_2-TPO analysis of the fresh and spent ZnO adsorbent.

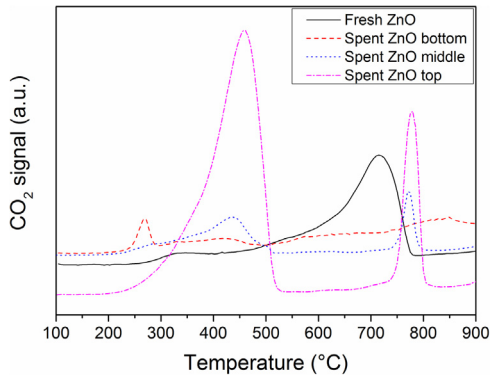

Fig. 7. CO_2-TPO analysis of the fresh and spent ZnO adsorbent.

tograms can be attributed to zinc aluminum carbonate hydroxide hydrate (ZACHH), aragonite ($CaCO_3$), and calcite ($CaCO_3$) which constitute the cement matrix of the adsorbent. The absence of their diffraction peaks in the spent sample suggests that they were probably washed out during CSCWG.

In Fig. 6, SO_2-TPO analysis shows a unique SO_2 desorption peak at ca. 700 °C for the three fractions, whereas no desorption peak occurred for the fresh adsorbent. The peak intensity differed according to the fractions and diminished with the length of the ZnO bed. This qualitative analysis demonstrated that ZnO was able to adsorb sulfur under SCW conditions. The concentration gradient of sulfur along the bed indicates that the mass transfer zone already reached the end of the ZnO bed meaning that sulfur must have been in contact with the catalyst.

In Fig. 7, several CO_2 desorption peaks were observed. The desorption peaks above 650 °C may be related to carbon species coming from the binders of the ZnO adsorbent which contained $CaCO_3$, whereas the desorption peaks at lower temperatures rather correspond to carbon deposits coming from the liquefied feed. Astonishingly, the top fraction of the ZnO bed contained more carbon deposits than the lower fractions. Perhaps the higher residence time for the top fraction was responsible for the larger amount of tars and/or coke formed in the ZnO bed.

The fresh and spent ZnO adsorbents were analyzed by carbon and sulfur elemental analysis to determine quantitatively their carbon and sulfur content (Table 5). The sulfur analysis showed a good correlation with SO_2-TPO analysis since a concentration gradient of sulfur along the ZnO bed was measured. Additionally, as observed by CO_2-TPO, the top fraction contained more carbon. Interestingly, the fresh ZnO contained a higher amount of carbon compared to the bottom and middle fractions. In accordance with the XRD measurements, the washing out of some carbon coming from the binders ($CaCO_3$) during CSCWG may be the reason.

Table 5
Carbon and sulfur elemental analysis of the fresh and spent ZnO adsorbents (dry basis).

Sample	C wt%[a]	S wt%[a]
Fresh ZnO	0.75 ± 0.01	0.04 ± 0.01
Spent ZnO bottom	0.27 ± 0.04	1.90 ± 0.08
Spent ZnO middle	0.52 ± 0.02	0.57 ± 0.03
Spent ZnO top	0.86 ± 0.04	0.52 ± 0.01

[a] Determined with C-S elemental analysis.

4. Conclusions

A commercial 5% Ru/C catalyst exhibited good catalytic performance during continuous CSCWG of *Chlorella vulgaris* over a period of 55 h. Characterization of the spent 5% Ru/C catalyst revealed that mainly sulfur poisoning was responsible for the deactivation of the catalyst. Coking, catalyst fouling by salt deposits, and Ru sintering have also contributed to the loss of catalytic activity but to a lesser extent. The implementation of a sulfur removal bed upstream of the catalytic bed was key for achieving the observed period of catalytic activity with this sulfur-rich feedstock. Sulfur species were chemically bound to a commercial ZnO adsorbent offering a protection of the catalyst from sulfur. Although the macroscopic structure of the adsorbent was well preserved, some changes of its physical structure and some signs of attrition were observed. Hence, further development of stable sulfur adsorbent materials is of interest for CSCWG technology.

Acknowledgements

This work was financially supported in the frame of the SunCHem project by the Competence Center Energy and Mobility (CCEM-CH), Swisselectric Research, and the Swiss Competence Center for Energy Research in Biomass, SCCER BIOSWEET. The authors would like to thank E. De Boni (SEM-EDX measurements, PSI), T. Käser (WDXRF and elemental analysis, PSI), F. Gramm (STEM measurements, ETHZ) and A. Wokaun (fruitful discussions, PSI).

References

[1] M. Gassner, F. Vogel, G. Heyen, F. Maréchal, Optimal process design for the polygeneration of SNG, power and heat by hydrothermal gasification of waste biomass: thermo-economic process modelling and integration, Energy Environ. Sci. 4 (2011) 1726.
[2] G. Peng, Methane production from microalgae via continuous catalytic supercritical water gasification: development of catalysts and sulfur removal techniques, in: PhD Thesis, École polytechnique fédérale de Lausanne, 2015, no. 6740.
[3] P. Azadi, E. Afif, F. Azadi, R. Farnood, Screening of nickel catalysts for selective hydrogen production using supercritical water gasification of glucose, Green Chem. 14 (2012) 1766.
[4] R.D. Cortright, R.R. Davda, J.A. Dumesic, Hydrogen from catalytic reforming of biomass-derived hydrocarbons in liquid water, Nature 418 (2002) 964–967.
[5] F. Vogel, Handbook of green chemistry, volume 2: heterogenous catalysis, in: R.H. Crabtree (Ed.), Handb. Green Chem., WILEY-VCH, Weinheim, 2009, pp. 281–324.
[6] D.J.M. De Vlieger, A.G. Chakinala, L. Lefferts, S.R.A. Kersten, K. Seshan, D.W.F. Brilman, Hydrogen from ethylene glycol by supercritical water reforming using noble and base metal catalysts, Appl. Catal. B-Environ. 111 (2012) 536–544.
[7] R.R. Davda, J.W. Shabaker, G.W. Huber, R.D. Cortright, J.A. Dumesic, Aqueous-phase reforming of ethylene glycol on silica-supported metal catalysts, Appl. Catal. B-Environ. 43 (2003) 13–26.
[8] M. Osada, O. Sato, M. Watanabe, K. Arai, M. Shirai, Water density effect on lignin gasification over supported noble metal catalysts in supercritical water, Energy Fuels 20 (2006) 930–935.
[9] P. Azadi, R. Farnood, Review of heterogeneous catalysts for sub- and supercritical water gasification of biomass and wastes, Int. J. Hydrogen Energy 36 (2011) 9529–9541.
[10] D.C. Elliott, M.R. Phelps, L.J. Sealock, E.G. Baker, Chemical-processing in high-pressure aqueous environments. 4. Continuous-flow reactor

process-development experiments for organics destruction, Ind. Eng. Chem. Res. 33 (1994) 566–574.
[11] D.C. Elliott, T.R. Hart, G.G. Neuenschwander, Chemical processing in high-pressure aqueous environments. 8. Improved catalysts for hydrothermal gasification, Ind. Eng. Chem. Res. 45 (2006) 3776–3781.
[12] H. Zöhrer, F. Mayr, F. Vogel, Stability and performance of ruthenium catalysts based on refractory oxide supports in supercritical water conditions, Energy Fuels 27 (2013) 4739–4747.
[13] G. Peng, C. Ludwig, F. Vogel, Ruthenium dispersion: a key parameter for the stability of supported ruthenium catalysts during catalytic supercritical water gasification, ChemCatChem 8 (2016) 139–141.
[14] A.G. Haiduc, M. Brandenberger, S. Suquet, F. Vogel, R. Bernier-Latmani, C. Ludwig, SunCHem: an integrated process for the hydrothermal production of methane from microalgae and CO_2 mitigation, J. Appl. Phycol. 21 (2009) 529–541.
[15] Q. Guan, C. Wei, P.E. Savage, Hydrothermal gasification of Nannochloropsis sp. with Ru/C, Energy Fuels 26 (2012) 4575–4582.
[16] M. Bagnoud-Velásquez, M. Brandenberger, F. Vogel, C. Ludwig, Continuous catalytic hydrothermal gasification of algal biomass and case study on toxicity of aluminum as a step toward effluents recycling, Catal. Today 223 (2014) 35–43.
[17] M.H. Waldner, Catalytic hydrothermal gasification of biomass for the production of synthetic natural gas, in: PhD Thesis, ETH, Zurich, 2007, No. 17100.
[18] M. Dreher, M. Steib, M. Nachtegaal, J. Wambach, F. Vogel, On-stream regeneration of a sulfur-poisoned ruthenium–carbon catalyst under hydrothermal gasification conditions, ChemCatChem 6 (2014) 626–633.
[19] D.C. Elliott, T.R. Hart, G.G. Neuenschwander, L.J. Rotness, M.V. Olarte, A.H. Zacher, Chemical processing in high-pressure aqueous environments. 9. Process development for catalytic gasification of algae feedstocks, Ind. Eng. Chem. Res. 51 (2012) 10768–10777.
[20] G. Peng, F. Vogel, D. Refardt, C. Ludwig, Catalytic supercritical water gasification: continuous methanization of Chlorella vulgaris, Algal Res. (2016), submitted.
[21] A. Borodzinski, M. Bonarowska, Relation between crystallite size and dispersion on supported metal catalysts, Langmuir 13 (1997) 5613–5620.
[22] M.H. Waldner, F. Krumeich, F. Vogel, Synthetic natural gas by hydrothermal gasification of biomass selection procedure towards a stable catalyst and its sodium sulfate tolerance, J. Supercrit. Fluids 43 (2007) 91–105.
[23] G. Peng, M. Steib, F. Gramm, C. Ludwig, F. Vogel, Synthesis factors affecting the catalytic performance and stability of Ru/C catalysts for supercritical water gasification, Catal. Sci. Technol. 4 (2014) 3329.
[24] M. Schubert, J.W. Regler, F. Vogel, Continuous salt precipitation and separation from supercritical water. Part 1: type 1 salts, J. Supercrit. Fluids 52 (2010) 99–112.
[25] M. Dreher, B. Johnson, A.A. Peterson, M. Nachtegaal, J. Wambach, F. Vogel, Catalysis in supercritical water: pathway of the methanation reaction and sulfur poisoning over a Ru/C catalyst during the reforming of biomolecules, J. Catal. 301 (2013) 38–45.